**RESEARCH**

# Seismic performance enhancement of RC framed structures through retrofitting and strengthening: an experimental and numerical study

Abdul Ghafar Wahab[1,2] · Tao Zhong[1,2] · Fangfang Wei[3] · Nadimullah Hakimi[4] · Dhiraj D. Ahiwale[5]

## Abstract

This study investigates the seismic performance of a two-bay, two-story reinforced concrete (RC) framed structure and proposes a retrofitting strategy by removing a column and strengthening the adjoining beams and columns using RC jacketing and post-tensioning tendons. Experimental testing and numerical simulations are conducted to assess the effectiveness of the retrofitting method. The experimental results indicate that the retrofitted RC frame exhibits enhanced lateral stiffness and shear force resistance, resulting in reduced shear deformation compared to the existing RC frame. However, the two frames' ductility and energy dissipation characteristics remain similar. Notably, failure in the retrofitted frame occurs primarily in the second-story beam–column joint, whereas the original frame experiences failure at the ground-floor beam–column joints. Furthermore, a numerical macro-based finite element model is developed in OpenSEES, validated with experimental data, and utilized for a parametric study. The numerical findings suggest that retrofitting is suitable when the axial compression ratio of the second story's side columns is kept below 0.52. Attention should be given to the size of the retrofitted columns to avoid compromising the upper floor's structural integrity, as the retrofitting process may result in a softer upper floor. It is essential to regulate the dimensions of retrofitted columns and ensure that the elastic lateral stiffness of the retrofitted story is greater than the upper story. In this case, a 350 and 300 mm column depth had acceptable performance. Overall, this study provides valuable insights into the seismic performance of retrofitted RC-framed structures. The findings emphasize the importance of appropriate column sizing and maintaining adequate lateral stiffness to enhance retrofitted buildings' structural integrity and seismic resistance.

**Keywords** Structural retrofitting · Strengthening · RC frame · Column removal · Post-tensioning · Crack pattern · Numerical simulation

✉ Abdul Ghafar Wahab
  ghafarw54@gmail.com

  Tao Zhong
  taozhong@kust.edu.cn

  Fangfang Wei
  weiff@hhu.edu.cn

  Nadimullah Hakimi
  Nadim.hakimi@gmail.com

  Dhiraj D. Ahiwale
  dhiraj.ahiwale@vpkbiet.org

1   Civil Engineering and Architecture Faculty, Kunming University of Science and Technology, Kunming 650500, China

2   Yunnan Earthquake Engineering Research Institute, Kunming 6505000, China

3   Civil Engineering and Transportation Engineering Faculty, Hehai University, Nanjing 2110024, China

4   Faculty of Material Science and Engineering, Kunming University of Science and Technology, Kunming 650500, China

5   Department of Civil Engineering, Vidya Pratishthan's Kamalnayan Bajaj Institute of Engineering and Technology, Baramati, SPPU, Pune 413133, India

# Introduction

With advancements in society and economics, the architectural demands placed on buildings in densely populated cities have evolved, necessitating additional space. Kaveh and Rahami (2006) investigated optimized structural design to increase precision and efficacy in utilizing materials. Kaveh (2014) stated that the method of finite elements can be utilized effectively for optimal structural analysis. After thoroughly investigating the correct seismic design of frame structures using numerous methodologies, it was determined that optimal structural design is cost effective (Kaveh and Nasrollahi, 2014). When assessing the static, dynamic, and stable behavior of symmetric and regular structures, Kaveh and Khayatazad (2013) focused on efficient approaches to identify Eigen solutions for matrices. The techniques apply to symmetric and regular structures and structures with additional or deleted members.

Retrofitting existing framed structures by removing columns and masonry walls has become a practical and cost-effective solution. However, if appropriate reinforcing measures are not implemented, the removal of columns can result in progressive collapse or intolerable deformations (Abdelrahman, 2023a; Huang et al., 2023; Lan et al., 2023; Yang et al., 2022; Zheng et al., 2022). Therefore, it is necessary to reinforce the beams located above the removed columns as well as the adjacent columns to ensure the structural stability of the building.

There are two commonly utilized methods for removing a column in structural retrofitting. The first approach involves converting the beam directly above the column into an underpinning beam, similar to a transfer girder. The second approach entails converting the stories directly above the removed column into truss systems (Yang et al., 2018). Various methods have been developed to enhance the flexural and shear resistance and the stiffness of underpinning beams. These methods include section enlargement, which involves increasing the cross-sectional area of reinforced concrete (RC).

Additionally, external prestressing or post-tensioning techniques can be employed, along with the use of externally attached plates (Abdelrahman, 2023b; Adhikary & Mutsuyoshi, 2006; Gläser & Löffler, 2018). The use of externally bonded plates and strips for structural strengthening has undergone notable advancements in recent years. It has progressed from steel plates to fiber-reinforced polymers (FRPs) and, more recently, to fabric-reinforced cementitious matrix composites. These advancements signify the continuous development and improvement in strengthening techniques (Al-Zaid et al., 2012; Matthys & Triantafillou, 2001). These materials, known for their high tensile strength, are applied to the tension side of structural components to improve their load-bearing capacity.

Additionally, strengthening RC columns through methods such as section enlargement using RC jacketing, or a combination of steel angles and battens, has gained popularity due to their effectiveness in enhancing strength and stiffness. Tarabia and Albakry (2014) investigated the strengthening of RC columns using steel angles (steel cage) and strips and observed an increased axial load capacity in the columns after reinforcement.

Campione (2012) conducted research comparing analytical formulations for calculating the load-bearing capacity of RC columns strengthened with steel strips and angles. The suggested formulations consider the contribution of transverse strip confinement effects to the overall strength. Salah et al. (2022) investigated the response of axially loaded L-shaped RC columns strengthened using steel jacketing. Such columns often require reinforcement in various scenarios, such as increased stories, changes in building function, design errors, or construction difficulties.

Currently, RC jacketing is the most widely used method for reinforcing and retrofitting weak or damaged RC columns (Habib et al., 2020). This method effectively restores and enhances reinforced concrete columns' stiffness and load-bearing capacity in earthquake-prone regions. The significance of this methodology lies in its capacity to significantly increase the load-carrying capacity, strength, and stiffness of any column section without necessitating specialized labor or time-consuming installation procedures. Furthermore, it provides uniform distribution of additional lateral resistance throughout the building (Akin & Sezer, 2016; Liu et al., 2016; Moustafa, 2012). The need for increased structural capacity in RC-framed structures arises from various factors, including seismic retrofitting, concrete degradation, design or construction errors, changes in building usage, and stricter code requirements (Chu et al., 2022; TahamouliRoudsari et al., 2019). Reinforcing concrete jacketing enables the augmentation of structural components beyond their initial state, which proves particularly valuable when the original strength is insufficient to support anticipated loads (Arya et al., 2014).

Several completed projects have successfully removed columns from existing buildings and retrofitted the beams and columns above the removed column and adjacent columns. Chu Mingjin (2007) proposed three strengthening schemes for Hongkou Hotel after removing a column: post-tensioning transfer beam, Vierendeel truss system, and steel braces. Aimin and Yanhe (2006) utilized the prestressed technique to retrofit a public building with a two-story basement and seven stories above, strengthening the beam above the removed column with external and internal prestressed strands. Pratik Shah (2016) used the preloading approach (post-tensioning method) to retrofit a 24-story

building by removing a column between the first and second floors. Although removing a column from an existing building and retrofitting the beams and columns above the removed column and adjacent columns have been implemented in several completed projects, there is still a limited amount of research and experimental studies investigating the seismic performance of retrofitted RC frame structures. Therefore, this study aims to conduct a static cyclic test and finite element analysis on a retrofitted RC framed structure after removing a column from the middle and retrofitting the beam above the removed column and neighboring columns using post-tensioning and RC jacketing.

The present study involves the construction of a two-bay, two-story retrofitted RC framed structure and an alternative RC frame for experimental assessment. The first specimen represents the existing RC frame, while the second represents the retrofitted RC frame after removing the middle column from the ground story. The beam above the removed and adjacent columns is strengthened using post-tensioning and RC jacketing. The specimens are subjected to steady vertical gravity and cyclic lateral loading throughout the testing process. The study comprehensively examines the seismic response of the two frames, considering factors such as failure mode, crack patterns, hysteresis loops, stiffness degradation, and energy dissipation capacity. The research includes developing and validating macro-based finite element models for parametric analyses. Based on the findings, suggestions regarding seismic behavior and recommendations for implementing reconstruction efforts are provided.

## Experimental program

In this section, the experimental program has been discussed in detail.

### Specimen design

The specimens used in this study were obtained from a four-story RC frame structure. The structure consisted of six spans and two bays, each span and bay length of 7.5 m. The overall height of the structural floor was 3.6 m. The columns had a cross-section size of $600 \times 600$ mm, while the beams had a cross-section size of $360 \times 600$ mm.

Regarding gravity loads, each story of the structure was subjected to a uniform load of 3.6 kN/m$^2$, while the roof had a uniform load of 2.0 kN/m$^2$. Furthermore, a live load of 2 kN/m$^2$ was accounted for in all stories. The structure was designed per the seismic design requirements specified in the Chinese national earthquake design code (GB50011, 2010). The building was situated in a seismic design Category II region, where the seismic design intensity was rated at 7 degrees. This intensity level corresponds to a maximum

ground acceleration of 0.1 g. These specifications ensure the structure represents a typical reinforced concrete frame in a seismic-prone area. This study aims to investigate the seismic performance of the retrofitted RC frame after column removal and reinforcement measures are implemented using samples from this structure.

### Existing frame specimen

A downscaled specimen of a two-bay, two-story RC frame was derived from the prototype structure, employing a 1:3 scaling factor. Figure 1 shows the geometric dimensions and reinforcement specifications of the original frame. The prototype structure had a span length of 2500 mm and a story height of 1200 mm. The beams possessed cross-sections measuring 120 mm in width and 200 mm in depth, while the columns had cross-sections of 200 mm in width and 200 mm in depth. An additional ground beam with $400 \times 450$ mm dimensions was constructed to ensure stability and provide a secure foundation. All structural elements were encased with a 20-mm-thick layer of concrete.

Figure 1 displays the reinforcement details, highlighting the configuration of longitudinal rebars in the beams and columns. Specifically, the beams' bottom and top longitudinal rebars comprised 2Ø10 bars, while the columns were reinforced with 4Ø10 bars. The spacing of stirrups was modified in the beams' plastic hinge zone. It ranged from Ø6 with an 80 mm center-to-center spacing to 160 mm in the middle span. Regarding the columns, Ø6@80 mm hoops were installed uniformly along their height.

### Retrofitted frame specimen

The first step to retrofit the existing RC frame involved removing the middle ground floor column and converting the two-bay beam into a transfer beam. The transfer beam was reinforced and strengthened by employing post-tensioning techniques and enlarging the RC section. These measures were implemented to ensure compliance with serviceability requirements and limit state design criteria. However, if the axial compression ratio of the removed middle column exceeded 0.3, the design approach indicated that the transfer beam would either need to be substantially larger, resulting in a significant decrease in ceiling height, or require excessive reinforcement without altering the section depth. As a result, utilizing the transfer beam to support the upper stories was only practical when the removed column had a minor axial compression ratio. Alternatively, options such as implementing a truss system transfer story or reinforcing the beams above the removed column on each story could be considered. In this particular design, the latter option was chosen.
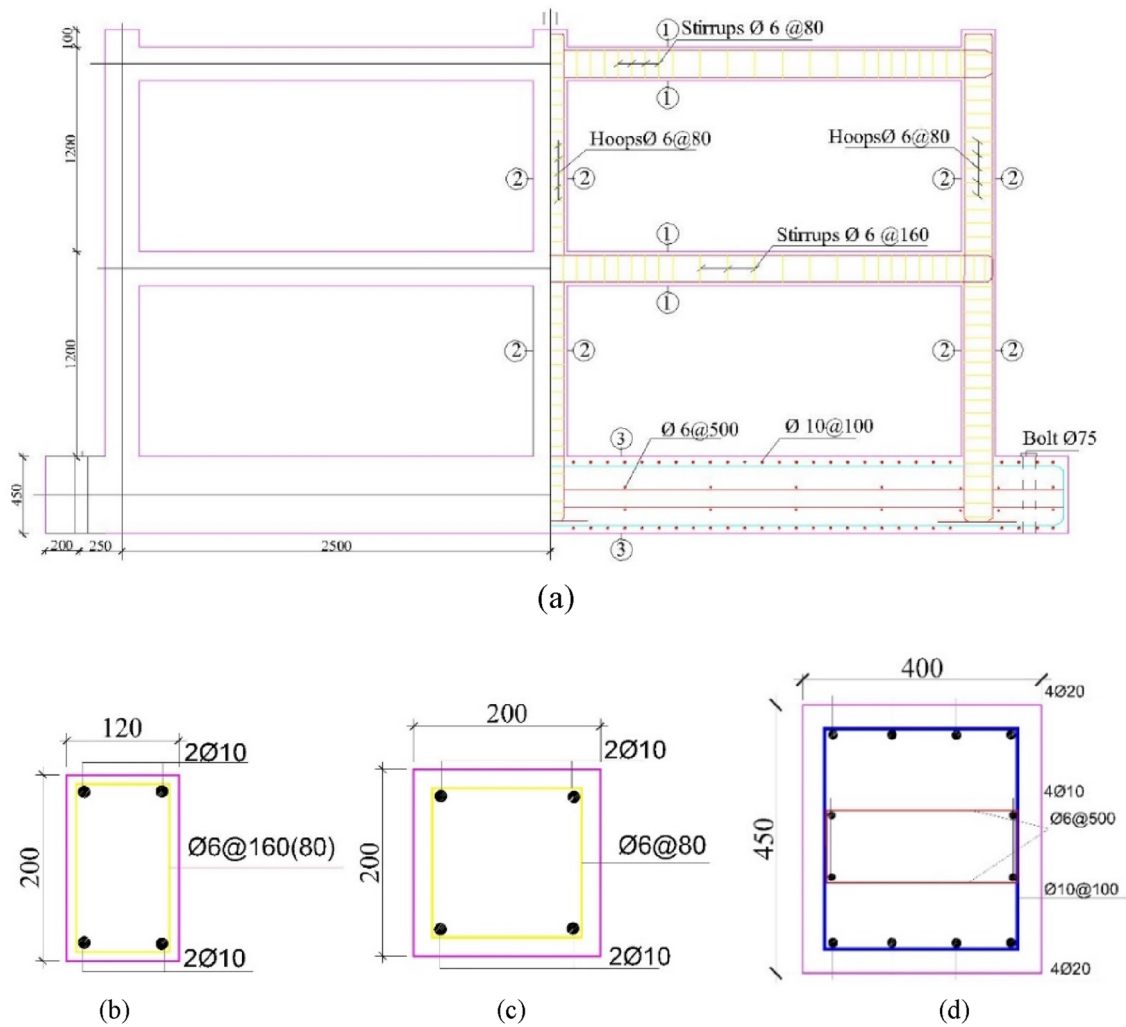
**Fig. 1** Existing RC frame specimen geometry and reinforcement details: **a** overall frame, **b** Sections 1–1, **c** Sections 2–2, and **d** Sections 3–3 (All units in millimeters)

Figure 2 illustrates the retrofitting scheme that was implemented, wherein a section of the load applied at the top of the middle column on the second story was directly transferred to the side columns of the ground floor. This transfer resulted in a substantial increase in the axial load borne by the side columns. To accommodate the load transmitted through the middle column of the second story, the ground-story beam acted as a transfer beam, experiencing the bending moment and shear force due to gravity. The beams, columns, and joints also needed reinforcement to enhance their lateral stiffness and prevent the ground story from becoming a soft story during horizontal seismic action.

To accomplish this objective, the design process encompassed the following essential steps:

1. A thorough evaluation of the beam's existing condition was carried out to ascertain the suitability of implement-

ing post-tensioning. This assessment aimed to determine if the beam was structurally sound and capable of supporting increased loads with the aid of post-tensioning.

2. The post-tensioning system was meticulously designed to meet the beam's required strength and load capacity. This entailed determining the optimal number and size of the tendons, selecting appropriate anchorage points, and establishing the necessary tensioning force. The post-tensioning tendons were employed in conjunction with an enlarged cross-section through scaling and additional reinforcing rebars. Typically, the tendons extending beyond the original section were anchored to the structure at designated anchor points, generally situated at the beam's ends.

3. A hydraulic jack was utilized to apply a gradual tensioning force to the tendons. It was crucial to incrementally
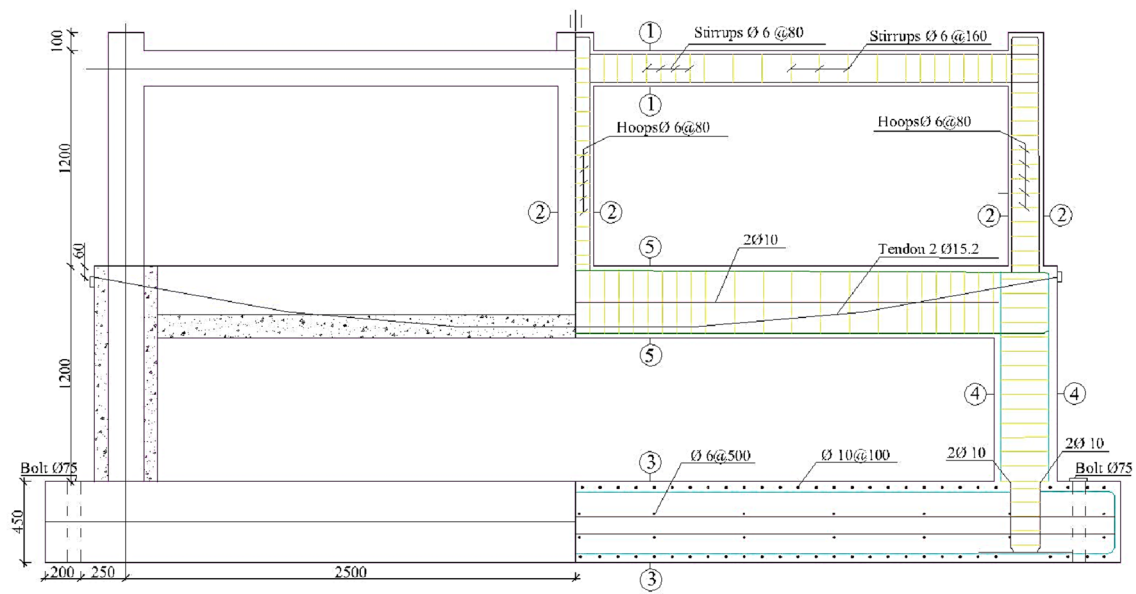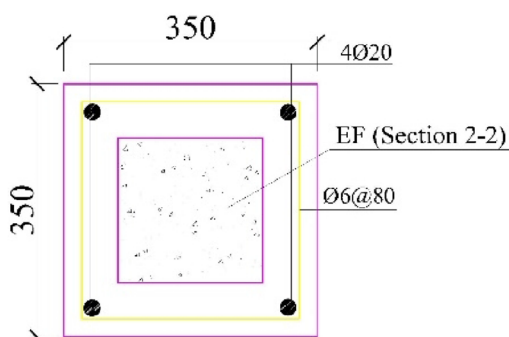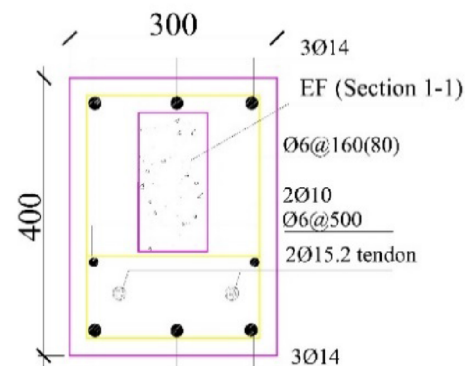
**Fig. 2** Geometric measurements and reinforcement detailing of the retrofitted RC frame specimen: **a** overall frame, **b** Sections 4–4, and **c** Sections 5–5 (All units in millimeters)

increase the tension force to prevent potential damage to the beam or tendons during the process.

4. The tendons were securely anchored at the beam's ends, generating a compressive force that enhanced the beam's structural capacity. Specialized anchor plates were employed for the tendon anchorage.

5. The cross-sectional dimensions of the two side columns supporting the transfer beam were enlarged using RC jacketing. This reinforcement technique was applied to enhance the lateral stiffness of the ground story, thereby increasing its resistance to horizontal forces.

Figure 2a showcases the retrofitted frame (RF) specimen, which closely resembles the existing frame (EF) specimen in terms of span length and story height. However, a notable distinction is observed in the ground story of the RF specimen, where the middle column has been eliminated. "The cross-section of the retrofitted column, achieved through RC jacketing, is presented in Fig. 2b. The retrofitted column includes 4Ø20 bars as longitudinal reinforcement and Ø6@80 mm stirrups. With an RC jacket of 75 mm thickness, the cross-section of the column has effectively increased to $350 \times 350$ mm. Moreover, the concrete and grouting materials used in the experiment exhibited compressive strengths of 31.1 MPa and 40.1 MPa, respectively, as determined through testing standard cubes. For further details regarding the material characteristics of the steel reinforcement, concrete, and steel strands, refer to Table 1."

**Table 1** Mechanical properties of materials

| Steel rebar | Diameter (mm) | Yield strength (MPa) | Ultimate strength (MPa) | Elastic modulus (MPa) |
|---|---|---|---|---|
| Ø 6 | 6 | 490.1 | 677.02 | $2.00 \times 10^5$ |
| Ø10 | 10 | 478.5 | 652.73 | $2.05 \times 10^5$ |
| Ø14 | 14 | 467.9 | 629.42 | $2.10 \times 10^5$ |
| Ø20 | 20 | 453.2 | 638.83 | $2.0 \times 10^5$ |
| Tendons | 15.2 | 1580 | 1860 | $1.95 \times 10^5$ |
| Concrete | Compressive strength $F\_cu$ (MPa) | 30.0 | | |
| Grouting material | | 40.0 | | |

Tension stress $\sigma = 0.7F_{yt} = 1302$ (MPa) was applied to the tendons to control the tension in the beam cross-section

## Test setup and instrumentation

Figure 3 illustrates the configuration of the cyclic test. "The specimens were anchored to the strong ground floor using high-strength bolts at both ends. Prior to applying horizontal loading, two rods were vertically prestressed between the strong foundation and a loading beam in each bay. The loading beam was supported by a spread beam at the top of the two columns. This setup allowed the prestressed load to be converted into vertical load acting on the top of the columns, resulting in an axial compression of 162 kN in the center column and 97 kN in the side columns. To prevent the vertical weight from affecting the horizontal movement of the frame, roller support was placed in the gap between the loading and spread beams. A servo-controlled hydraulic actuator with a loading capacity of 1000 kN was horizontally installed onto the reaction wall. This actuator was connected to the top of each specimen through loading plates secured by four horizontal rods.

As shown in the upper left inset of Fig. 3, a tension/compression load cell measuring 500 kN was positioned between the actuator and the loading plate to measure the applied horizontal load, whether in tension or compression. Displacement transducers, such as the one shown in the upper right inset of Fig. 3, were attached to the ends of the beams to measure the drift of each story. The data recording frequency was set at 0.5 Hz."



**Fig. 3** Cyclic loading test setup of the specimen
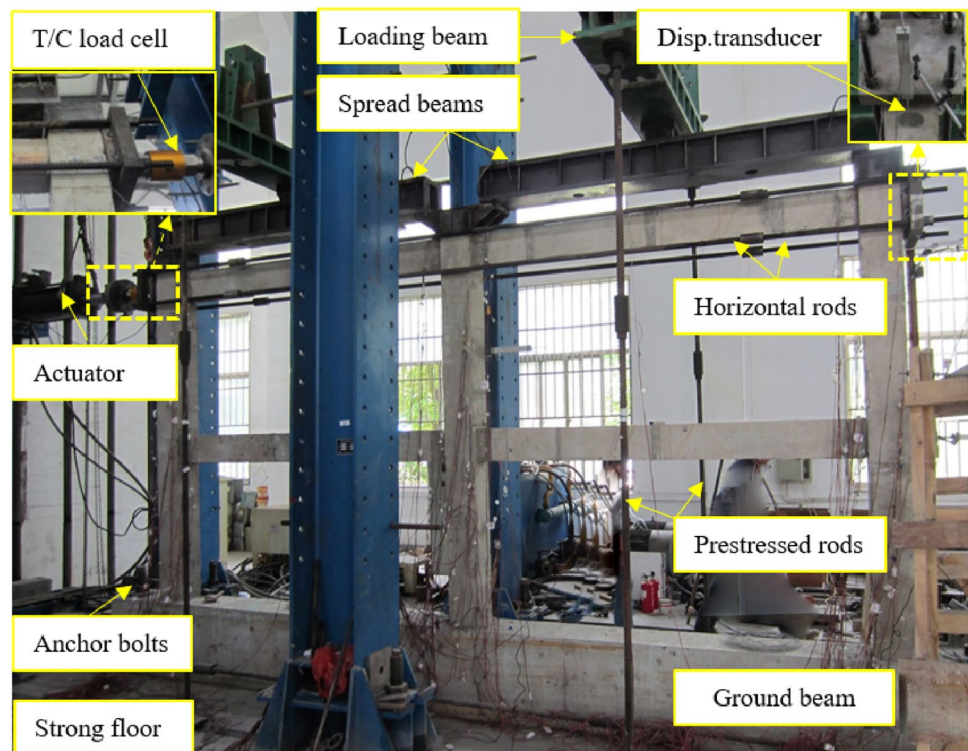
## The testing procedure and loading protocol

During each testing phase, the four vertical rods within each bay, as depicted in Fig. 3, were initially prestressed to induce the desired axial compressions in the middle and side columns. Subsequently, the specimens were subjected to horizontal cyclic loading until failure occurred. The axial compression ratios at the ground story's center and side columns, as per the original design of the RC frame, were 0.26 and 0.16, corresponding to axial compressions of 162 kN and 97 kN, respectively.

A quasi-static displacement control loading procedure was adopted to apply horizontal loading to the specimens, as shown in Fig. 4. "The loading displacement history was designed to incrementally increase the deformations experienced by the specimens throughout the test. At each displacement level, two complete reverse cycles were applied. Following the guidelines outlined in the specification for seismic testing of structures JGJ/T 101 (2015), the pre-yield displacement was increased in 2 mm increments until reaching the displacement corresponding to the yield of the structural resistance. Subsequently, the post-yield displacement was increased by estimated increments ($\Delta y$) until the point of failure, defined as the load being reduced to 85% of its peak value."

## Experimental results

When subjected to the loading conditions described in the preceding section, the primary failure modes observed in the specimens were localized at the beam–column connections. Specifically, failure occurred at the regions where plastic hinges formed in the beams and at the column ends. These critical locations experienced notable stress concentrations, making them susceptible to failure under the applied loading.

To accurately assess the seismic performance of the frames, two key experimental data sets are crucial: "the hysteresis behavior and the envelope curves. The hysteresis behavior provides valuable insights into the degradation of lateral stiffness and the energy-dissipation capability of the frames." The top portions of the hysteresis curves are particularly important, as they allow for the derivation of the frames' energy-dissipation capacity. By analyzing these curves, one can understand the deterioration of the frames' lateral stiffness and their ability to absorb seismic energy.

## Global behavior and local failure mechanism

### EF specimen

During the initial displacement cycle of 6 mm, with an applied force of 36.63 kN, minor cracks were observed on the right beam, indicating the initiation of localized damage. As the displacement increased to 8 mm, corresponding to a load of 43.6 kN, the first crack appeared at the right column of the ground story, indicating the onset of yielding in the column. Subsequently, additional cracks developed in both the left and right beams of the ground story, as evidenced by the crack patterns observed at a displacement of 16 mm in Fig. 5a.

At a displacement of 16 mm, strain gauge measurements indicated the first yield of the longitudinal reinforcement located at the right end of the ground-story beam. The displacement continued to increase until it reached a maximum of 32 mm. However, it was observed that the rate of load increase substantially decreased within the displacement range of 20–32 mm. This decrease in load increase rate was attributed to the crushing of concrete and the formation of plastic hinges at the beam ends. Consequently, after reaching the initial 32 mm displacement, subsequent displacements were incrementally increased at approximately 20 mm intervals for further testing and analysis.

**Fig. 4** Cyclic loading time history (mm)

(a)



(b)                                    (c)                                    (d)
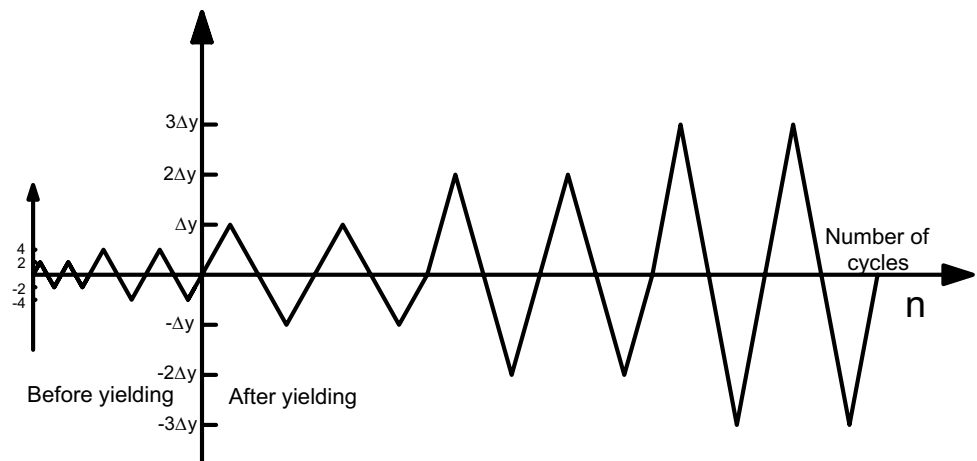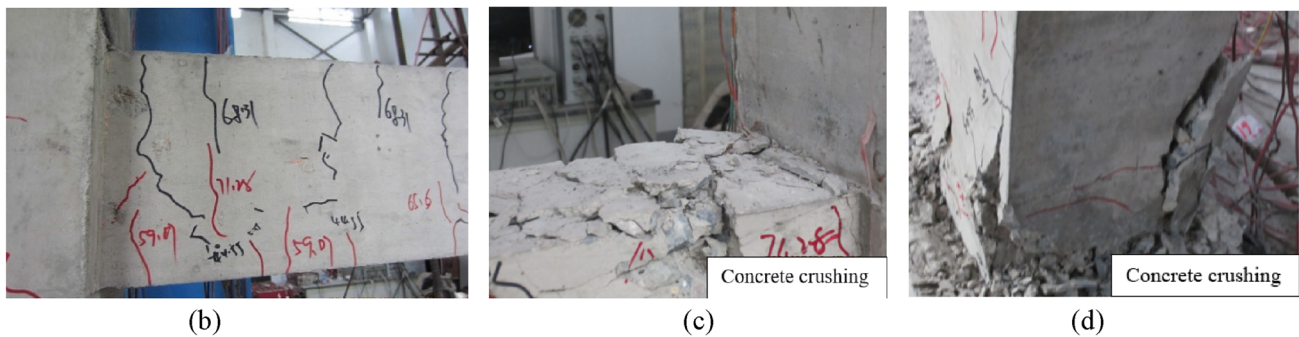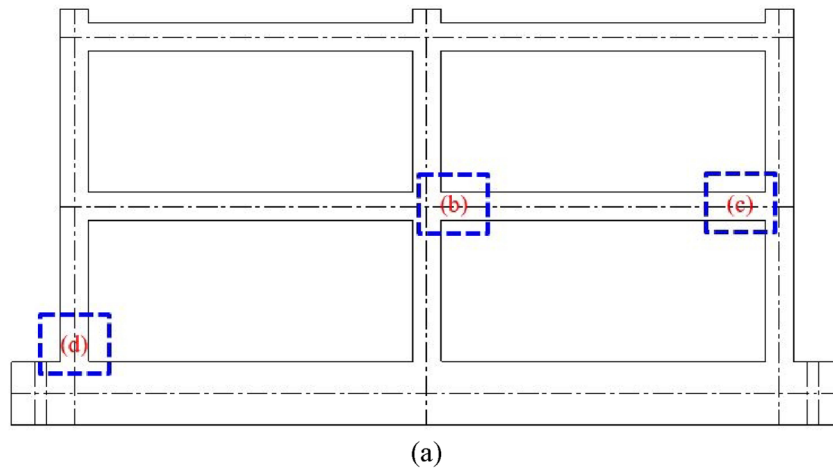
**Fig. 5** The EF specimen exhibited the following crack patterns and failure mechanisms: **a** the positions of localized failures; **b** the crack pattern at the end of the right beam at a lateral displacement of 16 mm; **c** the failure at the beam ends at a lateral displacement of 102 mm, including concrete spalling and stiffness degradation, and **d** the failure in the column at a lateral displacement of 102.2 mm, affecting the bottom ends

The maximum force of 95.04 kN was recorded at a displacement of approximately 48.82 mm. The test was terminated when the imposed displacement reached 102.2 mm, and the load dropped to 81.5 kN, representing around 85% of the peak load. Severe crushing of the concrete was observed at the beam ends, resulting in significant concrete spalling and degradation of the structural stiffness, as depicted in Fig. 5b. Similar crushing was observed at the first-story columns' bottom ends, as illustrated in Fig. 5c.

### RF specimen

Upon applying a vertical load to the specimen, no cracks were detected in the post-tensioned beam or any other structural components. This observation indicates that the retrofitted frame specimen operated within the normal functioning and serviceability limits.

During the horizontal loading process, the structure exhibited elastic behavior until reaching a displacement of 8 mm. However, as the displacement increased to 10 mm, the first crack emerged in both the right and left columns of the second floor, accompanied by a shear load of 99.09 kN. Subsequently, at a displacement of 12 mm, minor cracks appeared in the beam–column joints, coinciding with a load of 108.6 kN. Figure 6a illustrates these observations, depicting slight cracks in the strengthened post-tensioned beam and at the bottom of the strengthened ground story columns.

Following the 20 mm displacement, subsequent increments of 12 mm were imposed. The peak load of 132.27 kN was achieved at a displacement of approximately 36.24 mm. As the applied displacement reached 62.2 mm, the load decreased to 84.46 kN, which accounted for less than 85% of the maximum load. At this point, severe crushing of the concrete and buckling of longitudinal rebars were observed at the bottom of the second-story columns, as depicted in Fig. 6e. However, the ground story post-tensioned beam and columns remained within the serviceability state until the end of the test. This outcome underscores the effectiveness and efficiency of the retrofitting technique. Additionally, due to the failure of the second-story columns, the specimen experienced a significant decrease in stiffness, prompting the termination of the testing.
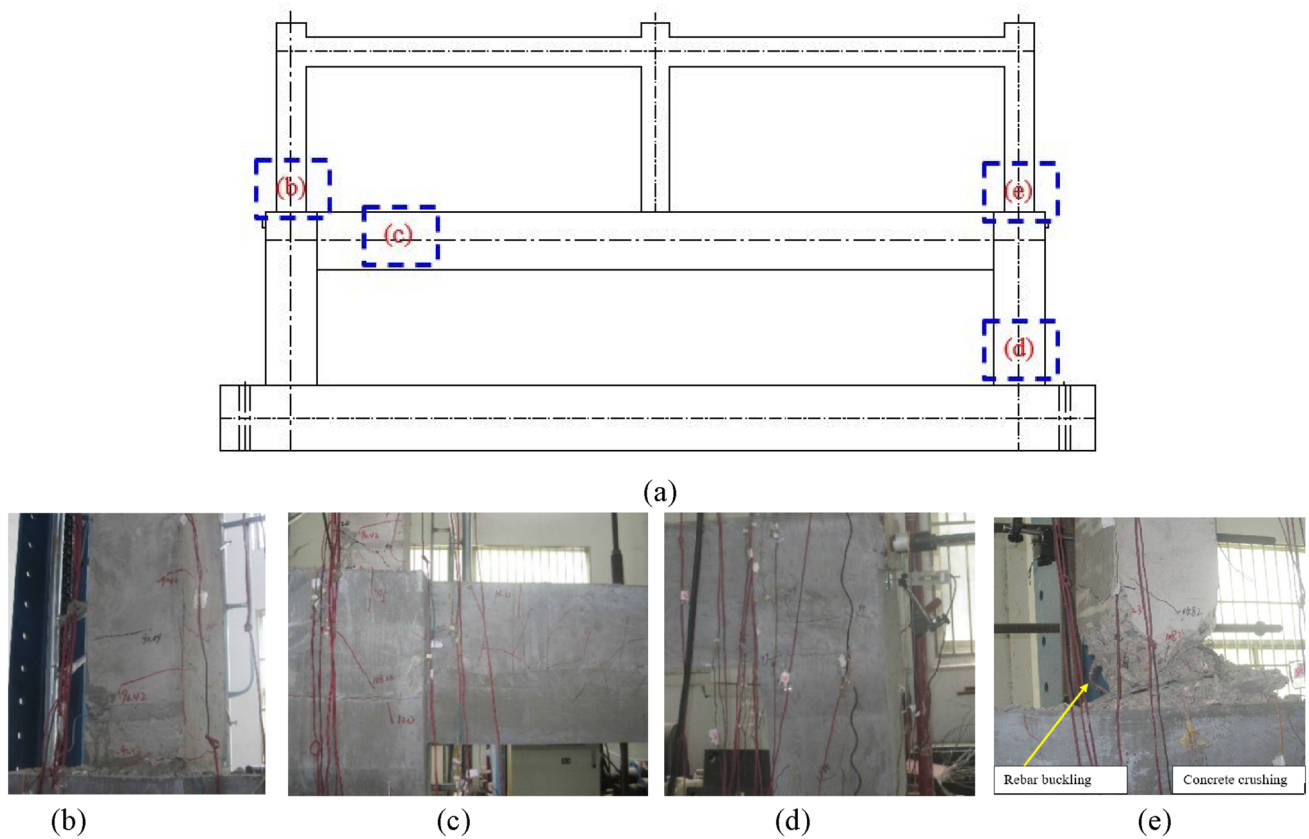
**Fig. 6** The crack patterns and failure mechanisms observed in the RF specimen are summarized as follows: **a** the positions of localized failures within the specimen; **b** the crack pattern observed at the end of the second-story column at a lateral displacement of 10 mm; **c** the crack pattern observed in the post-tensioned ground-story beam at a lateral displacement of 20 mm; **d** the crack pattern observed in the retrofitted column of the ground story, and **e** the failure of the second-story column and associated concrete spalling at a lateral displacement of 62.16 mm

## Hysteretic response and envelope curves

The hysteretic curve is an essential analytical tool for structural engineers to understand the behavior of a structure under cyclic loading. It plays a crucial role in evaluating the performance of a structure during seismic events or extreme conditions and guiding necessary improvements to enhance its resilience and safety. In this study, hysteretic curves of the EF and RF specimens were obtained and are presented in Fig. 7a, b. The observed hysteretic curves of both specimens exhibited similar characteristics. Initially, the response was elastic during the loading stage, with the loading stiffness closely resembling the unloading stage. The hysteretic curves displayed a shuttle-shaped pattern with a small, enclosed hysteresis loop area. As the displacement increased, the enclosed area of the hysteresis loop expanded, indicating an increase in energy dissipation by the specimens. The hysteresis loops exhibited a pinching phenomenon attributed to rebar slip, plastic hinge formation, and concrete cracking. Successive cycles of a specified displacement level reduced the specimens' stiffness and strength,

indicating material damage and beam–column joint failures. Specifically, severe damage was observed in the second-story column bottoms of the RF specimen, resulting in significant reductions in structural strength and stiffness within the hysteresis curve, particularly in the negative phase.

Envelope curves were generated by connecting the peak points of the first cycle's hysteretic curves at each loading level in the same direction. Figure 8a illustrates the envelope curves, which exhibited similar shapes in both positive and negative directions, indicating the symmetry of the shear performance of the specimens.

According to the specification for seismic testing of structures JGJ/T 101 (2015), various parameters such as the yield load ($P_y$), maximum load ($P_{max}$), ultimate load ($P_u$), and displacement ductility can be calculated from the envelope curve. Since the envelope curves did not exhibit a distinct yield point, the yield load ($P_y$) and corresponding yield displacement ($D_y$) were determined using the reciprocal area method, as shown in Fig. 8b. The peak load ($P_{max}$) corresponded to the maximum load on the envelope curve. In contrast, the ultimate load ($P_u$) accounted for

85% of the maximum load and corresponded to the ultimate displacement ($D_u$). The displacement ductility factor ($\mu$) of the specimens was defined as the ratio of ultimate displacement ($D_u$) to yield displacement ($D_y$). Table 2 provides an overview of the specimens' peak load, displacement characteristics, and ductility factor.

## Lateral stiffness degradation

During cyclic loading, the stiffness of specimens gradually decreases as the lateral displacement increases, a phenomenon referred to as stiffness degradation. Understanding stiffness degradation is essential for predicting structures and components' long-term performance and reliability in
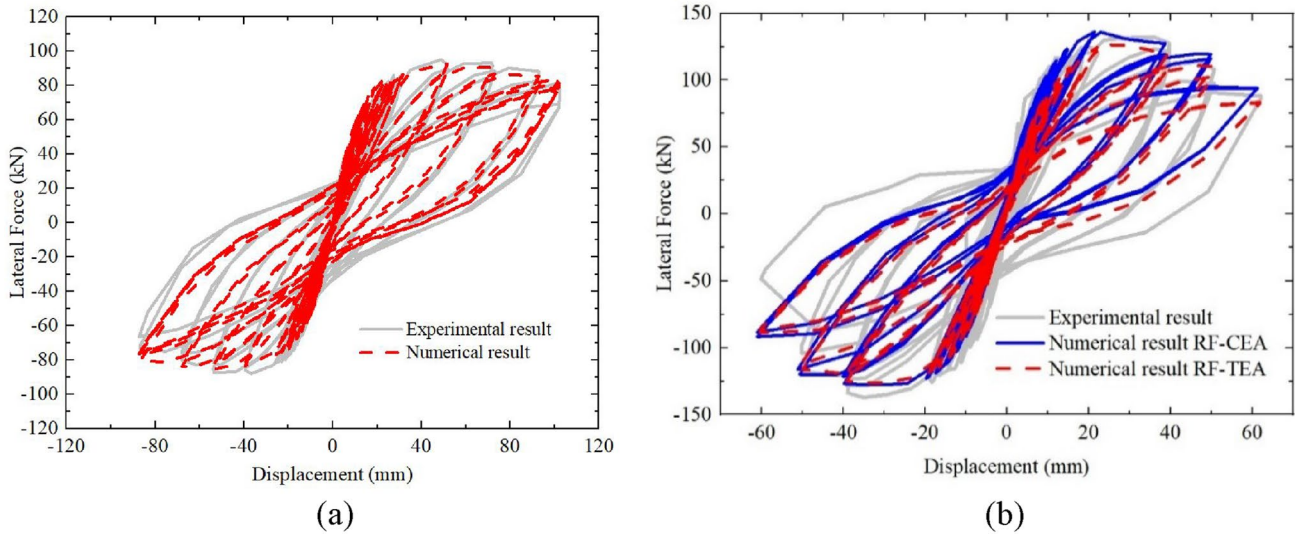


**Fig. 7** The hysteresis curves of the tested frame specimens: **a** The EF specimen and **b** The RF specimen
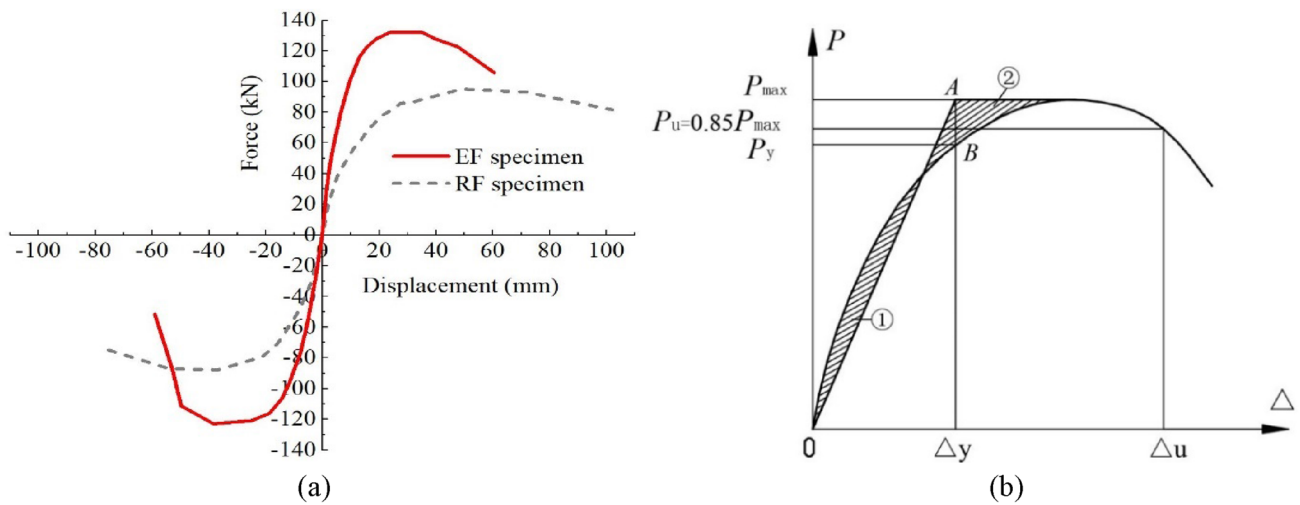


**Fig. 8** Envelope curve of the specimens: **a** envelope curve of the EF and RF specimen, and **b** principle of area reciprocity

**Table 2** Summary of the envelope curve and the ductility factor of the specimens

| Specimen | Yield point | | Peak point | | Ultimate point | | Ductility factor |
|---|---|---|---|---|---|---|---|
| | $P_y$ (kN) | $D_y$ (mm) | $P_{max}$ (kN) | $D_{max}$ (mm) | $P_u$ (kN) | $D_u$ (mm) | $\mu$ |
| EF | 75.64 | 19.29 | 95.04 | 48.82 | 80.78 | 102.11 | 5.29 |
| RF | 105.42 | 10.45 | 132.27 | 36.24 | 112.42 | 57.2 | 5.48 |

engineering design and analysis. The secant stiffness JGJ/T 101 (2015) is employed as a parameter to represent the specimens' stiffness at each loading stage and evaluate the stiffness degradation characteristics in RC frames under cyclic loading. The secant stiffness is calculated using Eq. (1).

$$K = \frac{|P_i| + |-P_i|}{|\Delta_i| + |-\Delta_i|}, \tag{1}$$

where $P_i$ and $-P_i$ are the lateral force of the specimen at the peak of the first cycle in each stage in the positive and negative directions, respectively, and $D_i$ and $-D_i$ are the corresponding lateral displacements in the positive and negative directions, respectively.

The evolution of stiffness degradation can be quantified and analyzed using the secant stiffness, providing valuable insights into the structural behavior and aiding in design considerations and retrofitting strategies. The secant stiffness $K$ and lateral displacement of the specimens are shown in Fig. 9. The RF specimens exhibited an initial (i.e., $K_{max}$) almost two times that EF specimen because of retrofitting measures. As the lateral displacement increased, the stiffness of both specimens exhibited a reduction. However, it was notable that the RF specimen demonstrated a faster rate of stiffness degradation than the EF specimen. This accelerated degradation can be attributed to the severe failure of the second-story columns at the bottom, which significantly impacted the overall stiffness of the RF specimen.

## Energy dissipation capacity

Energy dissipation in a structure is a crucial parameter determining its ability to absorb and dissipate energy during seismic events or cyclic loading (Abdul Ghafar et al., 2022a). It reflects the structure's capability to undergo

inelastic deformations while effectively reducing the transmitted energy. Evaluating the energy dissipation of specimens provides valuable insights into their seismic performance. The energy dissipation of the specimens can be quantified by measuring the area enclosed by the hysteretic loops (Abdul Ghafar et al., 2022b). This area represents the energy absorbed and dissipated during cyclic loading. Two commonly used metrics to assess energy dissipation are the energy dissipation coefficient ($E$) and the equivalent viscous damping coefficient $\zeta_e$ JGJ/T 101 (2015).

The energy dissipation of the specimens is measured from the area enclosed by the hysteretic loops using the energy dissipation coefficient $E$ or the equivalent viscous damping coefficients $\zeta_e$ JGJ/T 101 (2015). A larger enclosed area in the hysteretic loop indicates a higher value of $E$ or $\zeta_e$, signifying enhanced energy dissipation characteristics, and is calculated as:

$$E = \frac{S_{(ABC+CDA)}}{S_{(OBE+DOF)}}, \text{ or } \zeta_e = \frac{1}{2\pi} \frac{S_{(ABC+CDA)}}{S_{(OBE+DOF)}}, \tag{2}$$

where $S_{(ABC+CDA)}$ is the dissipated energy in a loading cycle on the hysteresis curve, and $S_{(OBE+DOF)}$ is the energy consumed by a linear elastic body equivalent to the specimen, defined by the areas surrounded by the triangles *OBE* and *DOF*, as shown in Fig. 10a.

In this study, the $\zeta_e$ was used to determine the energy dissipation capacity of both specimens, as shown in Fig. 10b. The EF specimen energy dissipation was measured higher than the RF specimen in the inelastic region, but both specimens exhibited the same energy dissipation in the elastic region. This information aids in designing and analyzing structures to ensure their resilience and ability to withstand seismic events.

## Numerical simulation

Due to the limited number of specimens available for testing and the need to thoroughly investigate the influential parameters of the renovated frame, a numerical analysis was conducted using a macro-based finite-element technique. This analysis aimed to explore the effects of these parameters and provide a comprehensive understanding of their impact on structural behavior.

For this purpose, the numerical analysis was performed using OpenSEES (Open System for Earthquake Engineering Simulation), an open-source software framework developed by McKenna (2011). OpenSEES is widely recognized and utilized in earthquake engineering due to its ability to simulate the behavior of structures subjected to seismic ground motions. It offers a robust platform for conducting accurate and reliable numerical simulations.
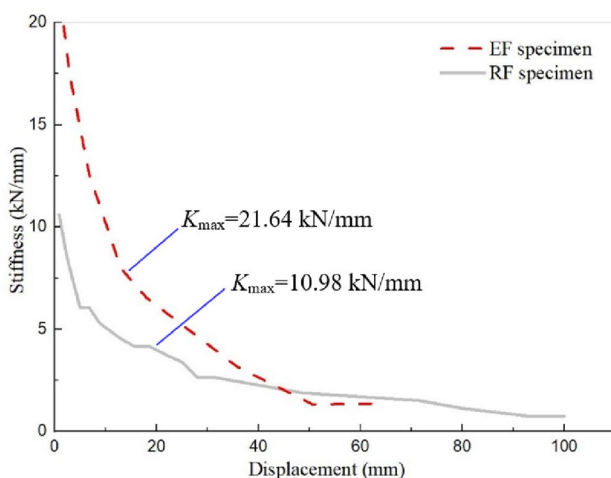


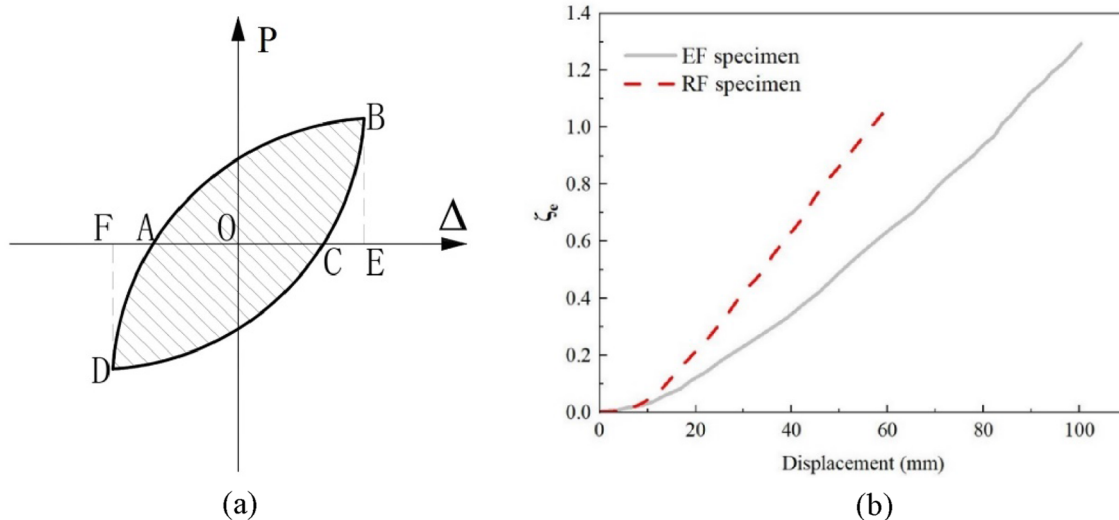**Fig. 9** Stiffness degradation curves

**Fig. 10** The energy dissipation of the specimens: **a** the definition of the energy dissipation coefficient, and **b** the energy dissipation coefficients of the EF and RF specimens

To validate the findings obtained from the experimental testing, finite element models of the tested specimens were developed within the OpenSEES platform. Figure 11a, b showcases the overall numerical models, denoted as Model-1 and Model-2, representing the EF and RF specimens, respectively. These models serve as valuable tools for further analysis and understanding of the structural response and performance under various loading scenarios. By combining experimental and numerical approaches, a comprehensive evaluation of the renovated frame's behavior and effectiveness can be achieved, contributing to improved design and retrofitting strategies.

## Numerical modeling techniques

### Element type

In the OpenSEES library, two element types are primarily employed for the accurate nonlinear modeling of reinforced concrete and steel structural elements. The first type is the force-based beam–column element, which employs an iterative force-based formulation. The second type is the displacement-based beam–column element, which adopts a displacement formulation and incorporates the spread of plasticity along the element (Balan et al., 1997; McKenna, 2011; Neuenhofer & Filippou, 1997). Displace-based fiber elements were used to model the retrofitted beam and columns, featuring ten Gauss–Legendre integration locations along their length. Meanwhile, force-based fiber elements were employed to represent the existing RC beam and columns, each comprising five Gauss–Legendre integration locations along its length. The section stress results at the

integration locations along each element were computed by discretizing the fiber section.

It was crucial to consider certain types of inelastic deformations to accurately capture the localized inelastic deformations at the member end regions and accurately represent the associated structural response and damage. One significant deformation observed in the beam–column interfaces is the fixed-end rotation of beams. This deformation occurs due to longitudinal bar slippage from the joint panels or one of the columns at the column-footing regions. Zero-length-section elements were incorporated into Model-1 at the beam end regions and the bottom of the ground-story columns to account for these effects. In contrast, zero-length-section elements were only added to the second-story columns and beams in Model-2, as the ground-story beam and columns were retrofitted and did not exhibit plastic hinge formation.

This approach ensured that the modeling accurately represented the observed deformations and behavior of the retrofitted structure. Each element with a zero-length section is defined by the force–deformation relationship specified by the section's properties.

### Post-tension tendons element modeling

In OpenSEES software, tendons can be modeled using two approaches depending on the level of detail and complexity required for the analysis (Lu et al., 2016; McKenna, 2011).

(1) Equivalent truss element approach: Tendons are modeled as equivalent nonlinear truss elements in this approach. The tendons are discretized into smaller segments, and the properties of each segment, such as

**Fig. 11** Numerical models of the specimens: **a** Model-1 for the EF specimen and **b** Model-2 for the RF specimen



(a)



(b)
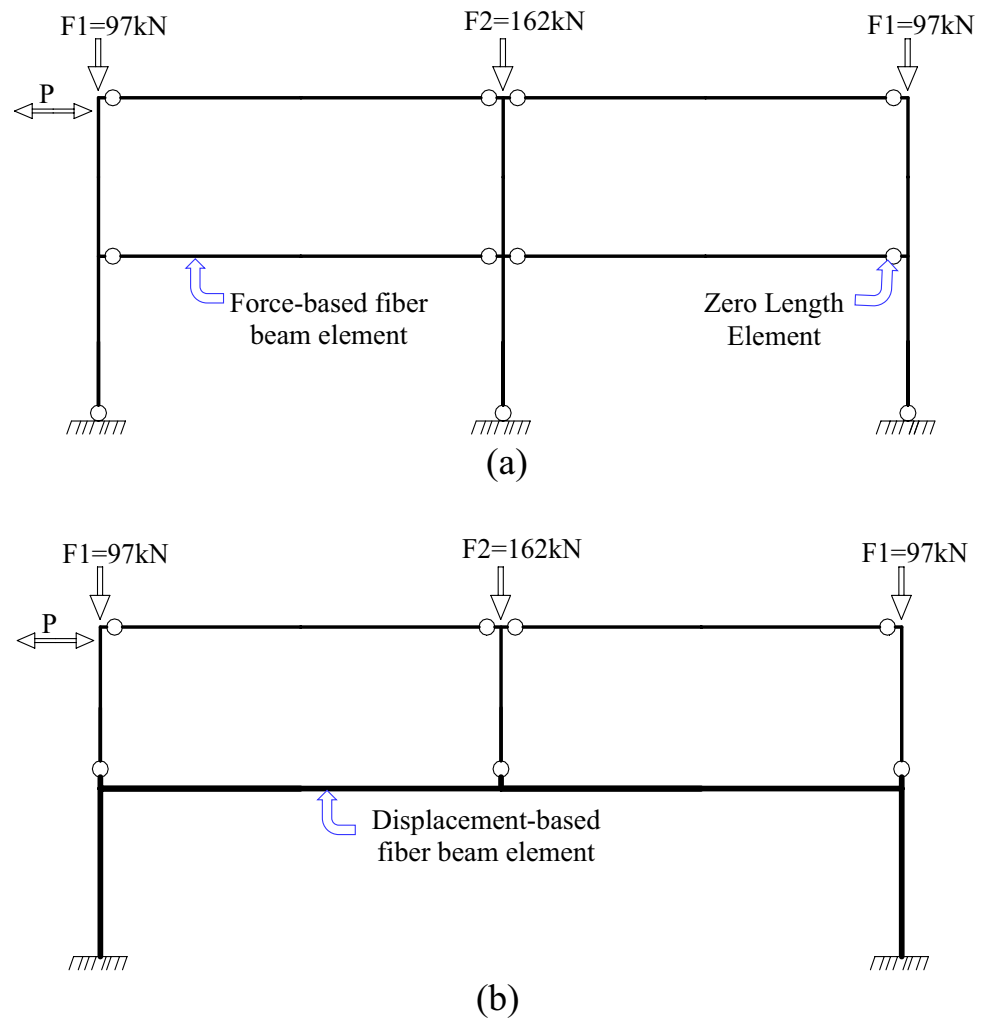
cross-sectional area, material properties, and prestress force, are assigned. Using appropriate boundary conditions, the equivalent truss elements are connected to the structural members they interact with, such as beams or columns. This approach provides a simplified representation of the tendon behavior and is suitable for preliminary analysis.

(2) Cable element approach: This approach involves modeling tendons as cable elements. Cable elements are specialized elements in OpenSEES that can represent the behavior of tension-only elements. Each tendon is defined as a series of interconnected cable elements, which can more accurately simulate the force–displacement relationship of the tendons. The cable elements consider the nonlinearity of the tendon material and can capture the effects of elongation, slip, and stress relaxation. This approach is more suitable for detailed analysis and can provide a more realistic representation of tendon behavior.

Both approaches require defining the material properties, prestress forces, and tendon geometry in the input file of the OpenSEES model.

This study utilized the equivalent truss and cable element approaches to model tendons in the OpenSEES software. The equivalent beam element approach was employed to simplify the tendon behavior in specific analyses. This approach discretized the tendons into smaller segments and assigned properties such as cross-sectional area, material properties, and prestress force. These equivalent truss elements were then connected to the structural members they interacted with, such as beams or columns.

Additionally, the cable element approach was implemented to capture the detailed behavior of the tendons in more comprehensive analyses. This approach modeled the tendons as a series of interconnected cable elements, taking into account the nonlinearity of the tendon material and considering effects such as elongation, slip, and stress relaxation. The cable elements provided a more accurate

representation of tendon behavior and were particularly useful for capturing the complex interaction between tendons and the surrounding structural elements.

By combining both approaches, this study examined tendon behavior at different levels of detail and complexity, allowing for a more comprehensive understanding of the structural response.

## Material model for concrete

In order to accurately represent the tensile strength contribution of concrete, the Concrete02 uniaxial material model from the OpenSEEs library (McKenna, 2011) is employed, as shown in Fig. 12. This model incorporates the phenomenon of linear tension softening that occurs during tensile loading. It also takes into account the influence of closed steel hoops on the confinement of concrete, allowing the concrete fibers to represent both confined and unconfined conditions. The compressive strength of confined concrete is 25.1 MPa, while the compressive strength of unconfined concrete is 30.73 MPa. By utilizing this material model, the behavior of concrete under various loading conditions can be accurately simulated and analyzed. "It is supposed that the elastic modulus of the tensile branch, denoted by the ($E_t$), has the value of to $E_t = f_t/0.002$, where $f_t = 0.70\sqrt{f'_c}$ is the tensile strength of the concrete, and $f'_c$, is the compressive strength of the concrete. The crushing strength measures out to be $0.40f'_c$. In addition to this, the ratio ($\lambda$) between the unloading slop should be determined. For confined and unconfined concrete, the strain at the compressive and crushing strengths is calculated as $-0.002$ and $-0.01$, respectively, and the $\lambda$ value is equivalent to 0.1."
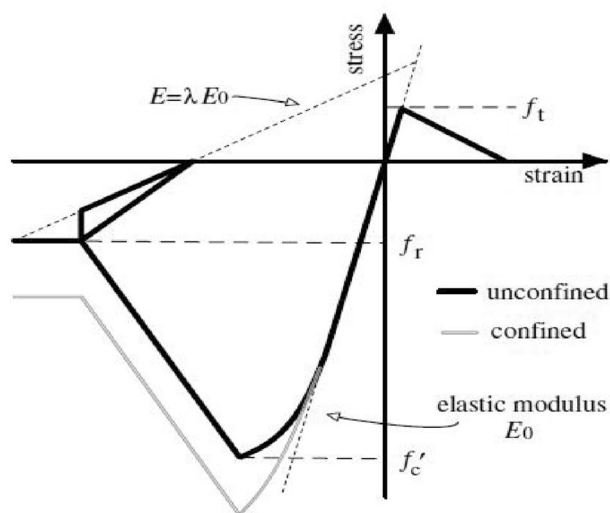
## Material model for steel and tendons

In order to accurately capture the pinching effect observed in hysteresis loops, a suitable constitutive model is required to characterize the behavior of the reinforcement steel and tendons. For this purpose, the uniaxial Menegotto-Pinto constitutive model, commonly known as Steel02, is employed in this study (McKenna, 2011). The Steel02 model incorporates linear kinematic hardening and zero isotropic hardening to accurately simulate the cyclic behavior of steel under varying loading conditions. This model is widely recognized for its ability to depict the pinched load-deformation response, which is characterized by strength and stiffness degradation as the material undergoes cyclic loading. By implementing the Steel02 model, the pinching effect in the hysteresis loops can be effectively captured, enabling a more realistic representation of the structural response under cyclic loading conditions.

## Material model for bond–slip

The Bond-sp01 "material model, proposed by Zhao and Sritharan (Zhao & Sritharan, 2007), is developed in OpenSEES to accurately represent the bond–slip behavior of steel reinforcement fibers in reinforced concrete (RC) member sections. This model considers the strain penetration at joint interfaces, providing a more realistic representation of the stress–slip relationship.

The stress–slip relationship in the Bond-sp01 model is shown in Fig. 13. The material strengths of the reinforcement fibers determine the yield stress and ultimate stress. It is important to note that the yield slip ($S_y$) and
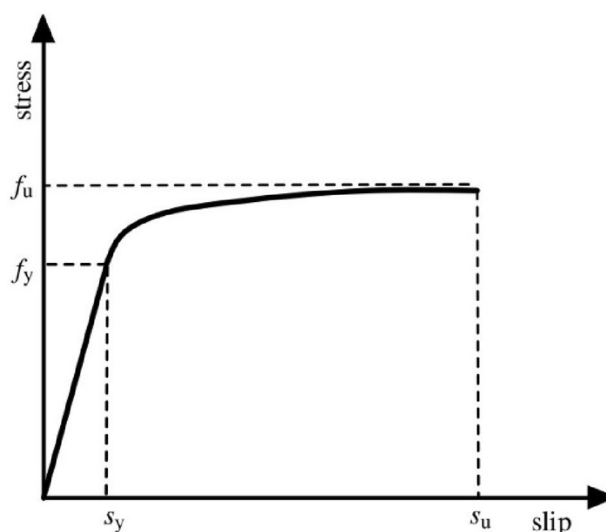


**Fig. 12** The uniaxial material Concrete02 stress–strain curve



**Fig. 13** Bond-sp01 material model stress–slip relationship (Zhao & Sritharan, 2007)

ultimate slip ($S_u$) must be calculated to fully characterize the model's behavior. Therefore, the $S_y$ is calculated from Eq. (3)."

$$S_y = 2.54 \left[ \frac{d_b}{8,437} \frac{\sigma_y}{\sqrt{F_c'}} (2\alpha + 1) \right]^{1/\alpha} + 0.34. \quad (3)$$

The Bond-sp01 model, proposed by Zhao and Sritharan (2007), considers key parameters in its formulation:$d_b$: Diameter of the longitudinal bars; $\sigma_y$: Yield strength of the longitudinal bars; $F_c'$: Compressive strength of the concrete$\alpha$: Parameter in the local bond–slip relation (typically set to 0.4). The ultimate slip ($S_u$) is assumed to be approximately 30 to 40 times the yield slip ($S_y$). This assumption estimates the slip value corresponding to the ultimate stress of the bond behavior.

These parameters and assumptions are important factors in accurately representing the bond–slip behavior between reinforcement fibers and concrete in the Bond-sp01 model.

## Analysis procedure in openSEES

A two-step analysis procedure is implemented in this research to evaluate the structure's behavior comprehensively.

Step 1's static analysis simulates the structure's response under specific loading conditions. An axial load is applied in the negative direction of the global y-axis on the top of the side columns, with a magnitude of 97 kN. Additionally, a load of 162 kN is applied to the middle column. The purpose of Step 1 is to investigate the structural response under static gravity loading and assess factors such as deformations, stresses, and load distribution.

Moving on to Step 2, a cyclic loading protocol replicates the same loading pattern used in the experimental study. This cyclic loading protocol aims to simulate the dynamic behavior experienced during seismic events. Numerical analysis can provide valuable insights into the structural response under seismic forces by applying the same loading pattern as the experiment. This step enables the evaluation of parameters such as displacement capacity, energy dissipation, and failure mechanisms.

The two-step analysis procedure allows for a comprehensive assessment of the structure's performance under both static and dynamic loading conditions. It facilitates a detailed understanding of the structural response to different loading scenarios, providing insights into the proposed retrofitting strategy's effectiveness and the structure's overall seismic performance.

## Verification of numerical simulation

Figure 7 compares the hysteresis curves obtained from experimental and numerical analyses for the two frame specimens. The hysteresis curves provide insights into structural resistance, stiffness, and hysteretic behavior variations. For specimen EF, it is evident that the numerical results closely match the experimental findings. The variations in structural resistance, stiffness, and hysteretic behavior show good agreement between the numerical and experimental results. For instance, the experimental maximum lateral force is measured at 95 kN, while the numerical result closely aligns with a value of 94 kN. The experimental and numerical findings exhibit remarkable agreement regarding the force levels observed at the maximum lateral displacement of approximately 100 mm. Furthermore, both the experimental and numerical analyses effectively capture the tested structure's pinching effect and energy-dissipation capacity. This close correlation between the experimental and numerical results confirms the reliability and accuracy of the numerical model in simulating the structural response under seismic loading conditions.

Regarding Specimen RF, as presented in Fig. 7b, the numerical results obtained from both the RF-CEA (cable element approach) and RF-TEA (truss element approach) demonstrate good agreement with the experimental results. However, it is worth noting that the cable element approach employed in RF-CEA provides a more accurate representation of the degradation of structural resistance as the lateral displacement increases.

The numerical results obtained from both approaches show reasonable agreement with the experimental data. However, the cable element approach, which models the behavior of the structural elements more precisely, captures the progressive deterioration of the structural resistance with increasing lateral displacement.

## Parametric study

The preceding experimental and numerical investigations have yielded compelling evidence supporting the feasibility of renovating RC frames by removing a column and the beam above it while implementing post-tensioned tendons and RC jacketing as a viable means to increase available space. Nevertheless, it is imperative to acknowledge the multifaceted nature of the renovation process, involving numerous parameters that necessitate a comprehensive examination of their impact on the quality of the renovation. This section addresses this research gap by conducting a parametric study employing a validated

numerical model. By systematically varying different parameters, this study aims to analyze their individual effects on the quality and effectiveness of the retrofitting method. The outcomes of these parametric studies will contribute significant insights into understanding the optimal values and combinations of parameters required for achieving successful renovations. Among the parameters under scrutiny, particular emphasis is placed on three key variables: "the Bottom Column Longitudinal Reinforcement Ratio (BCLRR), the Axial Compression Ratio of Columns (ACR), and the Section Depth of the Bottom Column (DBC)." These parameters play a pivotal role in determining the efficacy of the renovation process. A matrix of analysis cases, presented in Table 3, has been devised to explore their influence comprehensively. Importantly, all other parameters remain consistent with those utilized in the experimental tests. Through the systematic

variation and evaluation of these parameters, this research provides valuable insights and practical guidance to engineers and practitioners in renovation engineering. These findings will facilitate informed decision-making and aid in implementing optimal renovation strategies, ultimately advancing the state-of-the-art in this area.

### Effect of bottom column longitudinal reinforcement ratio

The effect of the longitudinal reinforcement ratio on the seismic performance of frame columns was investigated in this study. Reinforcement diameters of 10 mm, 14 mm, 16 mm, and 20 mm were considered, corresponding to reinforcement ratios of 1.3%, 2.6%, 3.25%, and 3.9%, respectively. It was found that increasing the longitudinal reinforcement ratio influenced the load–displacement behavior of the retrofitted

**Table 3** Different case studies on the seismic performance of frame columns

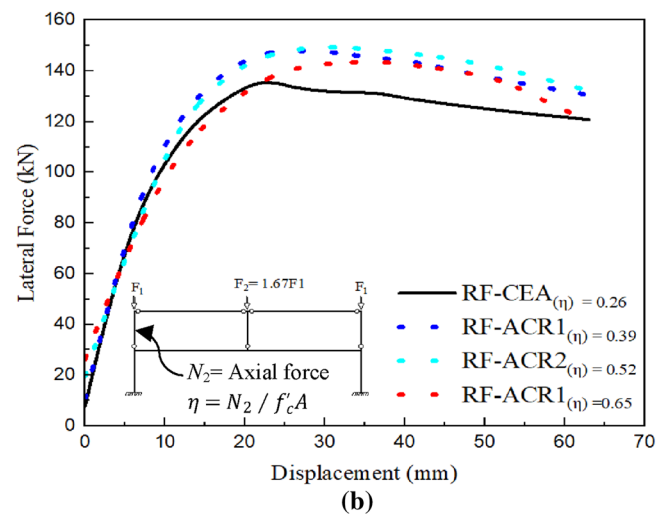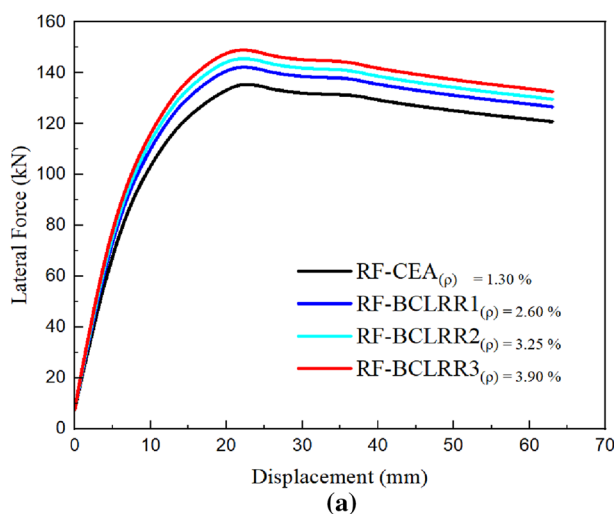| Case study | Column longitudinal reinforcement ratio $\rho$ (%) | Axial load compression ratio $\eta$ (%) | Retrofitted columns cross-section depth D (mm) |
|---|---|---|---|
| RF-CEA | 1.30 | 0.26 | 350 |
| RF-BCLRR 1 | 2.60 | 0.26 | 350 |
| RF-BCLRR 2 | 3.25 | 0.26 | 350 |
| RF-BCLRR 3 | 3.90 | 0.26 | 350 |
| RF-ACR 1 | 1.30 | 0.39 | 350 |
| RF-ACR 2 | 1.30 | 0.52 | 350 |
| RF-ACR 3 | 1.30 | 0.65 | 350 |
| RF-DBC 1 | 1.30 | 0.26 | 250 |
| RF-DBC 2 | 1.30 | 0.26 | 300 |
| RF-DBC 3 | 1.30 | 0.26 | 400 |



**Fig. 14** Lateral force–displacement response of the retrofitted frame: **a** with varying bottom columns longitudinal reinforcement ratios, and **b** with varying axial compression ratios

structure, as depicted in Fig. 14a. Table 3 shows the different case studies on the seismic performance of frame columns.

The results revealed that higher longitudinal reinforcement ratios improved several structural parameters. Specifically, the yield load, yield displacement, peak load, and peak displacement showed noticeable enhancements with an increase in the reinforcement ratio. Notably, even a slight increase in amplitude was observed when the reinforcement ratio reached 3.9% compared to a ratio of 1.3%. These findings indicate that increasing the column's longitudinal reinforcement ratio can enhance the structure's seismic performance within a limited range.

However, it is essential to consider that the effectiveness of this approach may vary depending on specific design requirements and structural configurations. Other factors, such as anticipated seismic forces and overall structural design, should also be considered when determining the optimal reinforcement parameters to achieve desired seismic performance and ensure structural safety.

### Section depth of the bottom column effect

The removal of a column leads to the redistribution of the axial load, which is initially borne by the adjacent columns. Consequently, the corresponding axial compression ratio increases. "Adhering to the Chinese seismic design code (GB50011, 2010), it is imperative to maintain the axial compression ratio within specified limits to ensure the desired ductility for each designated design category. Moreover, enhancing the lateral story stiffness is necessary to prevent the renovated (ground) story from becoming soft, especially in buildings with limited bays. One practical approach is to employ reinforced concrete (RC) jacketing, which involves increasing the column section dimensions. Therefore, the investigation focuses on studying the impact of the renovated story column depth, assuming a square section, on the overall structural response.

According to Fig. 15b, it is evident that there is a slight enhancement in structural stiffness and resistance when the dimensions (D) of the bottom column sections are increased. Based on Fig. 15b, it can be observed that as the sections become smaller, the deformation tends to concentrate more quickly on the renovated story, even during the elastic stage." Comparing the D = 350 and D = 400, there is no significant change in the load bearing; therefore, it is revealed that D = 350 and D = 300 is suitable.

## Conclusions

This study aimed to develop a post-tensioning and concrete jacketing technique for retrofitting and upgrading RC framed structures after column removal. To achieve this objective, two specimens were examined under a cyclic loading system to investigate the seismic behaviors of the renovated frame (RF) and the existing frame (EF). The EF specimen consisted of a two-bay, two-story RC frame with axial loads applied to each column in the upper story. Meanwhile, the RF specimen represented the renovated RC frame, also with a two-bay, two-story configuration, where axial loads were applied to each column in the upper story. Under cyclic loading, the seismic behavior of each specimen was thoroughly investigated. Various parameters were analyzed, including hysteresis behavior, envelope curves, energy dissipation,
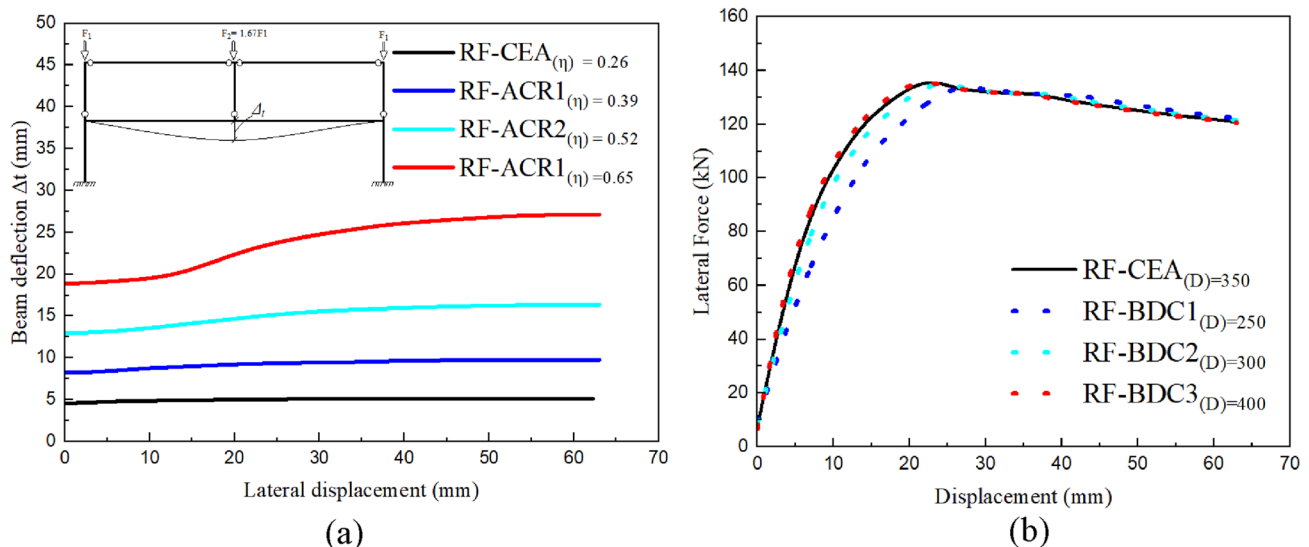


**Fig. 15** **a** Lateral displacement and the corresponding vertical deflection of the post-tensioned beam, and **b** Lateral force–displacement response of the retrofitted frame with varying bottom column depth

ductility, and stiffness degradation capacities. These results were plotted and described to understand the structural response comprehensively.

The study's findings revealed that the renovation method significantly influenced the retrofitted structure's structural strength, load-carrying capacity, and seismic performance. Furthermore, all specimens were subjected to numerical investigations using the Finite Element program OpenSEES. The obtained numerical results were then compared with the available experimental data. Additionally, a parametric analysis was conducted to assess the impacts on the overall structural behavior, providing further insights into the effectiveness of the retrofitting measures. The main conclusions drawn from the study are as follows:

1. The post-tensioning method and concrete jacketing used for retrofitting and upgrading the RC framed structure after column removal demonstrated significant improvements in structural strength, load-carrying capacity, and seismic performance. Comparing the load bearing of RF improved by 40% than the existing frame, and the RF had minor deformation but slightly higher ductility than the EF. The energy dissipation capacity of RF and EF were observed to be similar.
2. The study revealed that the renovated frame exhibited a smaller deformation capacity than the original structure. This reduction in deformation capacity was primarily attributed to the failure of the bottom of the second-story column and the buckling of longitudinal rebars.
3. Based on the study's findings, it is strongly recommended that the renovation technique be cautiously employed and carefully considering the axial compression ratio of the side columns at the upper story. It is advised to ensure that the axial compression ratio of the side columns does not exceed 0.52.
4. It was determined the retrofitted bottom column's depth could impact the structure's lateral stiffness; when the D is reduced to 250 mm, the elastic stiffness quickly changed, and the force–displacement curve showed very softening in the elastic region. The parametric study revealed that D with 300 and 350 mm performed excellently.

The current research efforts primarily focus on applying renovation techniques in the context of two-bay two-story frames. However, future work should emphasize extending these techniques to multibay multistory structures.

## Declarations

## References

Abdelrahman, A. (2023). Strengthening of concrete columns. *Strengthening of concrete structures: unified design approach, numerical examples and case studies* (pp. 35–85). Springer Nature Singapore. https://doi.org/10.1007/978-981-19-8076-3_2

Abdelrahman, A. (2023). *Strengthening of concrete structures: unified design approach, numerical examples and case studies*. Springer Nature.

Abdul Ghafar, W., Tao, Z., Tao, Y., He, Y., Wu, L., & Zhang, Z. (2022). Experimental and numerical study of an innovative infill web-strips steel plate shear wall with rigid beam-to-column connections. *Buildings, 12*(10), 1560. https://doi.org/10.3390/buildings12101560

Abdul Ghafar, W., Zhong, T., Abid, M., Faizan, E., Mohamed, A., & Yosri, A. M. (2022b). Seismic performance investigation of an innovative steel shear wall with semi-rigid beam-to-column connections [Original Research]. *Frontiers in Materials*. https://doi.org/10.3389/fmats.2022.1075300

Adhikary, B. B., & Mutsuyoshi, H. (2006). Shear strengthening of reinforced concrete beams using various techniques. *Construction and Building Materials, 20*(6), 366–373. https://doi.org/10.1016/j.conbuildmat.2005.01.024

Aimin, Y., & Yanhe, L. (2006). Strengthen design for removal column and extending span by using the prestressed structure with same tendon located internally and externally. *Journal of Building Structures, 36*(11), 9–12.

Akin, A., & Sezer, R. (2016). A study on strengthening of reinforced concrete frames using precast concrete panels. *KSCE Journal of Civil Engineering, 20*(6), 2439–2446. https://doi.org/10.1007/s12205-016-0188-z

Al-Zaid, R. Z., Al-Negheimish, A. I., Al-Saawani, M. A., & El-Sayed, A. K. (2012). Analytical study on RC beams strengthened for flexure with externally bonded FRP reinforcement. *Composites Part B: Engineering, 43*(2), 129–141. https://doi.org/10.1016/j.compositesb.2011.11.015

Arya, A. S., Boen, T., & Ishiyama, Y. (2014). Guidelines for earthquake resistant non-engineered construction. UNESCO

Balan, T. A., Filippou, F. C., & Popov, E. P. (1997). Constitutive model for 3D cyclic analysis of concrete structures. *Journal of Engineering Mechanics, 123*(2), 143–153. https://doi.org/10.1061/(ASCE)0733-9399(1997)123:2(143)

Campione, G. (2012). Load carrying capacity of RC compressed columns strengthened with steel angles and strips. *Engineering Structures, 40*, 457–465. https://doi.org/10.1016/j.engstruct.2012.03.006

Chu Mingjin, S. Z. (2007). Structural design on column removing of hongkou hotel. *Journal of Building Structures, 37*, 26–28.

Chu, Y., Zhong, Y., Shi, B., & Gong, Y. (2022). Experimental study on seismic performance of seismic-damaged RC frames strengthened by different strengthening methods. *Structures, 41*, 1475–1487. https://doi.org/10.1016/j.istruc.2022.05.103

GB50011. (2010). Code for seismic design of buildings. National Standards of the People's Republic of China. https://www.chinestandard.net/PDF.aspx/GB50011-2010

Gläser, C., & Löffler, K. (2018). Post-tensioning Systems for the Strengthening of Structures. High Tech Concrete: Where Technology and Engineering Meet: Proceedings of the 2017 fib Symposium, held in Maastricht, The Netherlands, June 12–14, 2017

Habib, A., Yildirim, U., & Eren, O. (2020). Column repair and strengthening using RC jacketing: a brief state-of-the-art review. *Innovative Infrastructure Solutions*. https://doi.org/10.1007/s41062-020-00329-4

Huang, X., Elchalakani, M., Yu, P., Lin, R., Nie, Y., & He, S. (2023). Progressive collapse resistance of steel frame with beam to column transfer structure under a middle column-removal scenario. *Structures, 51*, 1–12. https://doi.org/10.1016/j.istruc.2023.03.041

JGJ-101. (2015). Specification of testing methods for earthquake resistant building

Kaveh, A. (2014). *Computational structural analysis and finite element methods*. Springer. https://doi.org/10.1007/978-3-319-02964-1

Kaveh, A., & Khayatazad, M. (2013). Ray optimization for size and shape optimization of truss structures. *Computers & Structures, 117*, 82–94.

Kaveh, A., & Rahami, H. (2006). Nonlinear analysis and optimal design of structures via force method and genetic algorithm. *Computers & Structures, 84*(12), 770–778. https://doi.org/10.1016/j.compstruc.2006.02.004

Kaveh, A., & Nasrollahi, A. (2014). Charged system search and particle swarm optimization hybridized for optimal design of engineering structures. *Scientia Iranica, 21*(2), 295–305.

Lan, X., Li, Z., Fu, F., & Qian, K. (2023). Robustness of steel braced frame to resist disproportionate collapse caused by corner column removal. *Journal of Building Engineering, 69*, 106226. https://doi.org/10.1016/j.jobe.2023.106226

Liu, C., Shi, J., Hiroshi, K., Taguchi, T., & Kamiya, T. (2016). Experiment study on RC frame retrofitted by the external structure. *Earthquake Engineering and Engineering Vibration, 15*(3), 563–574. https://doi.org/10.1007/s11803-016-0344-y

Lu, L., Tadepalli, P. R., Mo, Y. L., & Hsu, T. T. C. (2016). Simulation of prestressed steel fiber concrete beams subjected to shear. *International Journal of Concrete Structures and Materials, 10*(3), 297–306. https://doi.org/10.1007/s40069-016-0153-8

Matthys, S., & Triantafillou, T. (2001). Shear and torsion strengthening with externally bonded FRP reinforcement. In Composites in Construction: A Reality. pp. 203–212

McKenna, F. (2011). OpenSees: A framework for earthquake engineering simulation. *Computing in Science & Engineering, 13*(4), 58–66. https://doi.org/10.1109/MCSE.2011.66

Moustafa, A. (2012). Earthquake-resistant structures: design, assessment and rehabilitation. IntechOpen. https://books.google.fr/books?id=vAWaDwAAQBAJ

Neuenhofer, A., & Filippou, F. C. (1997). Evaluation of nonlinear frame finite-element models. *Journal of Structural Engineering, 123*(7), 958–966. https://doi.org/10.1061/(ASCE)0733-9445(1997)123:7(958)

Pratik Shah, P. E., Leed AP. (2016). Preloading Approach to Column Removal in an Existing Building. Structure Magazine

Salah, A., Elsanadedy, H., Abbas, H., Almusallam, T., & Al-Salloum, Y. (2022). Behavior of axially loaded L-shaped RC columns strengthened using steel jacketing. *Journal of Building Engineering, 47*, 103870. https://doi.org/10.1016/j.jobe.2021.103870

TahamouliRoudsari, M., Torkaman, M., Entezari, A. R., Rahimi, H., & Niazi, K. K. (2019). Experimental investigation of strengthening reinforced concrete moment resisting frames using partially attached steel infill plate. *Structures, 19*, 173–183. https://doi.org/10.1016/j.istruc.2019.01.009

Tarabia, A. M., & Albakry, H. F. (2014). Strengthening of RC columns by steel angles and strips. *Alexandria Engineering Journal, 53*(3), 615–626. https://doi.org/10.1016/j.aej.2014.04.005

Yang, J.-M., Kim, J.-K., & Yoo, D.-Y. (2018). Transfer length in full-scale pretensioned concrete beams with 1.4 m and 2.4 m section depths. *Engineering Structures, 171*, 433–444. https://doi.org/10.1016/j.engstruct.2018.05.104

Yang, T., Chen, X., Zhang, Y., Li, X., & Han, Z. (2022). Numerical analysis on collapse performance of post-tensioned concrete frames with post-tensioning BFRP bars under an interior-column-removal scenario. *Structures, 41*, 1288–1300. https://doi.org/10.1016/j.istruc.2022.05.051

Zhao, J., & Sritharan, S. (2007). Modeling of strain penetration effects in fiber-based analysis of reinforced concrete structures. *ACI Structural Journal, 104*(2), 133.

Zheng, L., Wang, W.-D., & Li, H.-W. (2022). Progressive collapse resistance of composite frame with concrete-filled steel tubular column under a penultimate column removal scenario. *Journal of Constructional Steel Research, 189*, 107085. https://doi.org/10.1016/j.jcsr.2021.107085